ACS OMEGA

http://pubs.acs.org/journal/acsodf

Article

3D/2D Heterojunction of CeO_2/Ultrathin MXene Nanosheets for Photocatalytic Hydrogen Production

Hongrui Zhu,* Xumei Fu, and Zhiqiang Zhou

Cite This: *ACS Omega* 2022, 7, 21684−21693

Read Online

ACCESS | Metrics & More | Article Recommendations | Supporting Information

ABSTRACT: Two-dimensional (2D) nanomaterials benefit from the high specific surface area, unique surface properties, and quantum size effects, which have attracted widespread scientific attention. MXenes add many members to the 2D material family, mainly metal conductors, most of which are dielectrics, semiconductors, or semimetals. With excellent electron mobility, beneficial to electron−hole separation, and large functional groups that can be tightly coupled with other materials, MXenes have broad application prospects in photocatalysis. Meanwhile, the application of CeO_2-based materials in organic catalysis, photocatalytic water splitting, and photodegradation of organic pollutants has been extensively explored, and studies have found that CeO_2-based materials show good photocatalytic performance. In view of this, we synthesized regular octahedral CeO_2 with a homojunction in one step by a hydrothermal method and compounded it with ultrathin 2D material MXene, which exhibited fast carrier migration efficiency and a good interfacial effect, making the material show excellent photocatalytic activity. The results showed that the photocatalytic H_2 evolution performance of the MXene/CeO_2 heterojunction was significantly improved. In this study, a low-cost catalyst with high photocatalytic activity was prepared, presenting a new research idea for achieving a combined 3D/2D photocatalytic system.

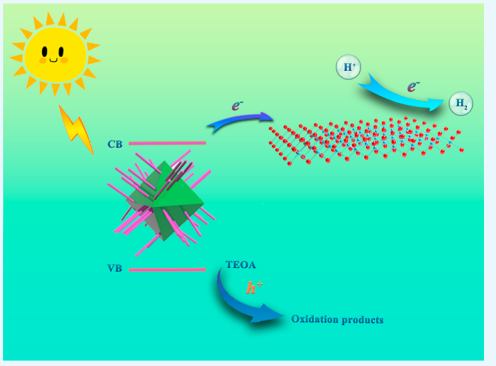

1. INTRODUCTION

The massive global energy consumption has led to severe environmental problems. People urgently need a clean energy source to solve the increasingly severe ecological problems. Photocatalytic hydrogen production is one of the ideal ways to harness solar energy to solve the growing energy crisis and environmental problems.[1,2] To date, using semiconductor photocatalysts to decompose water to produce hydrogen is one of the most attractive methods of solar energy conversion. The critical points of the practical application of photocatalytic H_2 evolution technology are high efficiency, high stability, and low cost.[3−5] However, one of the modification methods to improve the hydrogen production performance of the catalyst system is to synthesize various noble metals, such as Pt, Pd, Au, Ag, etc., on the surface. However, the cost consumed in the actual production of a photocatalyst is exceptionally high, and at the same time, heavy metals pollute the environment to a certain extent. Therefore, the exploration of non-precious metal catalysts is significant for achieving improved photocatalyst performance to split water to produce hydrogen.[6,7]

As the most abundant rare earth oxide, n-type cerium oxide (CeO_2) is widely used in high-efficiency photocatalysts because of its ease of converting Ce^{4+} to Ce^{3+}. Cerium dioxide (CeO_2) is a widely utilized catalyst material because of its excellent photocatalytic performance, simple synthesis method, and environmental friendliness.[8,9] Typically, non-semiconductor catalysts exhibit superior photocatalytic activity and reaction stability after forming heterojunctions with CeO_2.[10,11] With the recent research on rare earth metal oxides, there has been many reports in the literature on the modification of CeO_2 materials to improve their photocatalytic activity. Li et al. studied the activity and stability under different reaction conditions by synthesizing the exposed surface of CeO_2 nanoparticles with a controllable shape.[12] Jiang et al. investigated the non-homogeneous reactivity of CeO_2 NCs with different crystalline surface shapes in other photocatalytic processes. They found that surface defect structures (e.g., Ce^{3+} ions and O vacancies) significantly affected the surface properties of CeO_2 nanomaterials.[13] Zheng et al. successfully synthesized CeO_2 nanocrystals with specific shapes with clear crystal faces and a hierarchical porous structure.[14]

Two-dimensional materials are excellent complexes for the construction of CeO_2-based heterojunctions because of their excellent optical and electrochemical performances.[15] MXene is a new type of two-dimensional transition metal carbide/

Received: March 19, 2022
Accepted: June 7, 2022
Published: June 16, 2022

Scheme 1. Illustration of the Controllable Synthesis of CeO_2 and CeO_2/MXene

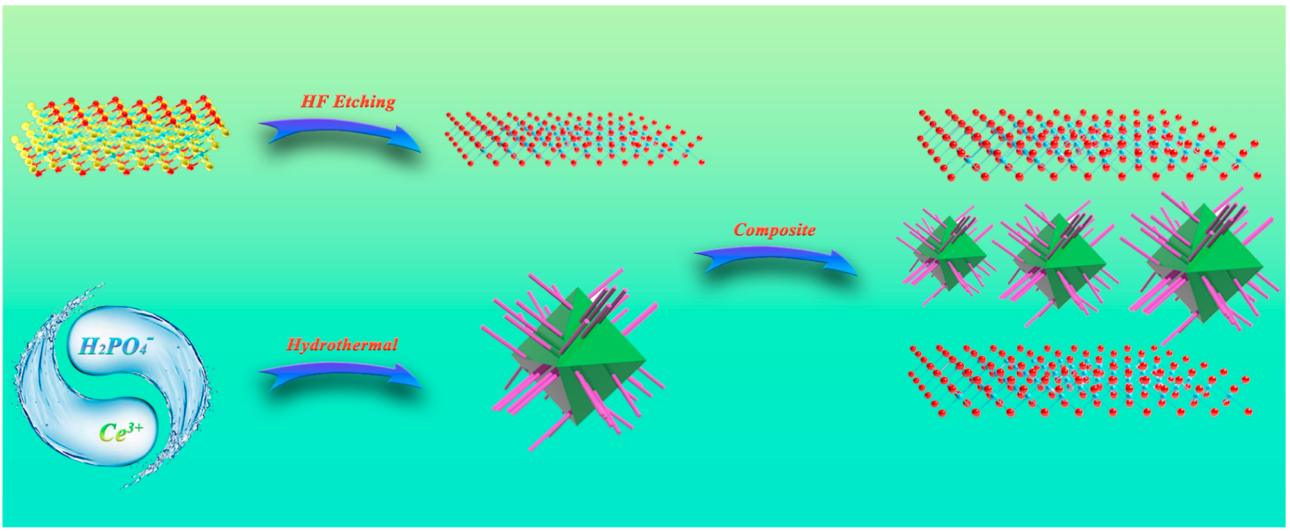

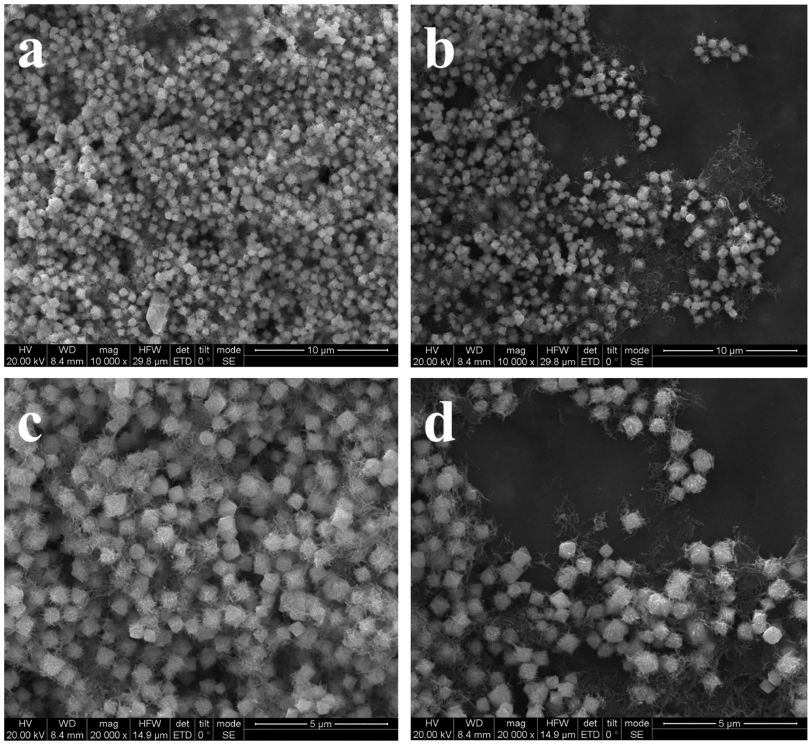

Figure 1. Low-magnification (a,b) and high-magnification (c,d) SEM images of hexahedral prism-anchored octahedral CeO_2.

carbonitride/nitride, which has attracted more and more attention since the discovery of Ti_3C_2 in 2011.[16,17] MXenes are usually obtained by selective etching of the MAX phase (M stands for transition metals, A stands for IIIA/IVA elements, and X stands for C/N elements).[18] On the one hand, MXenes have excellent carrier mobility, a large specific surface area, and many active sites, leading to a large number of reactions occurring on the surface, reducing the carrier migration distance. On the other hand, MXenes have good elasticity and a unique layered structure, making them easy to compound on other photocatalyst surfaces.[19] MXenes also show excellent potential in photocatalysis and can be used as a synergistic catalyst because the above advantages can effectively separate/transfer light-induced carriers and many active surface sites for catalytic reactions.[20,21] Owing to the ideal photoresponsiveness and electronic coupling properties, the migration efficiency of photo-generated electron−hole pairs at the heterojunction interface is improved, which can greatly enhance the photocatalytic activity of the material.[22] Recently, it has been reported that ideal nanostructures and good interfacial effects between materials are more likely to accelerate the migration rate of photo-generated carriers and thus improve the catalytic activity of PHE.[23]

In this study, a 2D MXene/3D CeO_2 photocatalyst was successfully prepared by synthesizing hexahedral prism-anchored octahedral CeO_2 and compounding a thin layer of two-dimensional material MXenes on the surface. This photocatalyst has the advantages of being non-toxic and

https://doi.org/10.1021/acsomega.2c01674
ACS Omega 2022, 7, 21684−21693

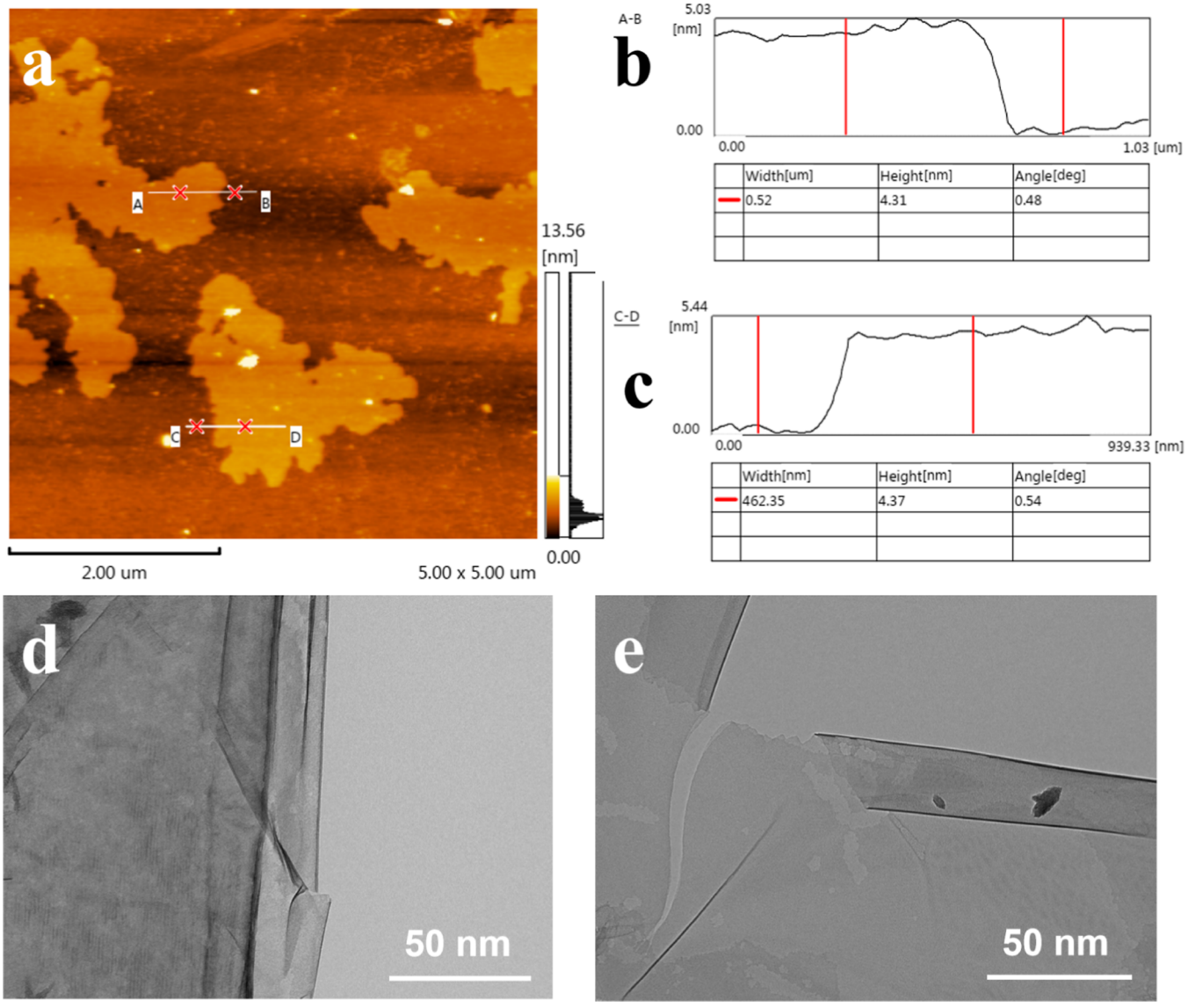

Figure 2. AFM (a–c) and FETEM (d,e) images of MXene.

harmless and a simple synthesis method. The highest yield of photocatalytic H_2 evolution is 454.32 μmol·g^{-1}·h^{-1}. Finally, the possible reaction mechanism of photocatalytic H_2 evolution is explained. The increase in photocatalytic activity may be due to the interface effect of 2D/3D materials, resulting in many active sites on the surface of the material. This work provides new ideas and directions for researching other 2D/3D heterojunction photocatalyst materials.

2. EXPERIMENTAL SECTION

2.1. Materials. The whole chemicals used in this research were obtained from commercial suppliers and used without further distillation. Ti_3AlC_2 (Macklin, 98%), $NaH_2PO_4{\cdot}2H_2O$, $Ce(NO_3)_3{\cdot}6H_2O$, DMSO, and hydrofluoric acid (HF, content ≥40.0%) were supplied by Aladdin Reagent Co., Ltd.

2.2. Synthesis of Ti_3C_2 Nanosheets. Ti_3C_2 nanosheets were prepared according to the method reported elsewhere with some modifications.[6] 1.0 g of Ti_3AlC_2 powders were immersed in 20 mL 40% HF aqueous solution and stirred at room temperature (RT) for 72 h to etch out Al in Ti_3AlC_2. The suspension was filtrated, rinsed with deionized water until the pH of the supernatant became near 7, and then dried at 80 °C for 12 h. To achieve the exfoliation, the obtained multilayered Ti_3C_2 powder was added to 20 mL DMSO and stirred for 24 h. The mixture obtained was centrifuged and washed with deionized water more than three times to obtain a solid powder. The collected solid powder was then dispersed into deionized water again and layered by ultrasonication. After ultrasonication for 1 h, the suspension was removed by centrifugation at 5000 rpm for 1 h to remove the unexfoliated Ti_3C_2. Finally, the supernatant of Ti_3C_2 nanosheets was obtained.

2.3. Synthesis of Hexahedral Prism-Decorated CeO_2 Octahedron. Referring to the method synthesized by Zou et al., hexahedral prism-anchored octahedral CeO_2 was synthesized.[24]

2.4. Preparation of CeO_2–$Ti_3C_2T_x$ MXene. First, multilayered Ti_3AlC_2 two-dimensional material was synthesized, and Ti_3AlC_2 was etched into few-layer MXene nanosheets by adding hydrofluoric acid and ultrasonic treatment.[25] Second, according to the reported method to synthesize hexahedral prism-anchored octahedral CeO_2, a certain amount of CeO_2

https://doi.org/10.1021/acsomega.2c01674
ACS Omega 2022, 7, 21684–21693

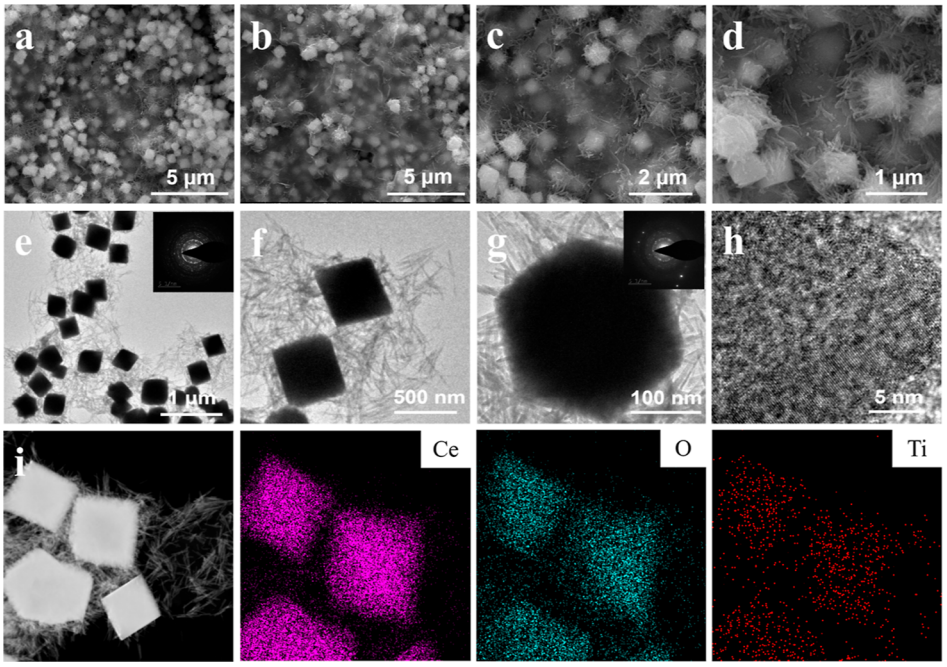

Figure 3. SEM images of CeO_2/MXene (a–d), TEM images of CeO_2/MXene (e–h), and the element maps of Ce, O, and Ti of the selected area (i).

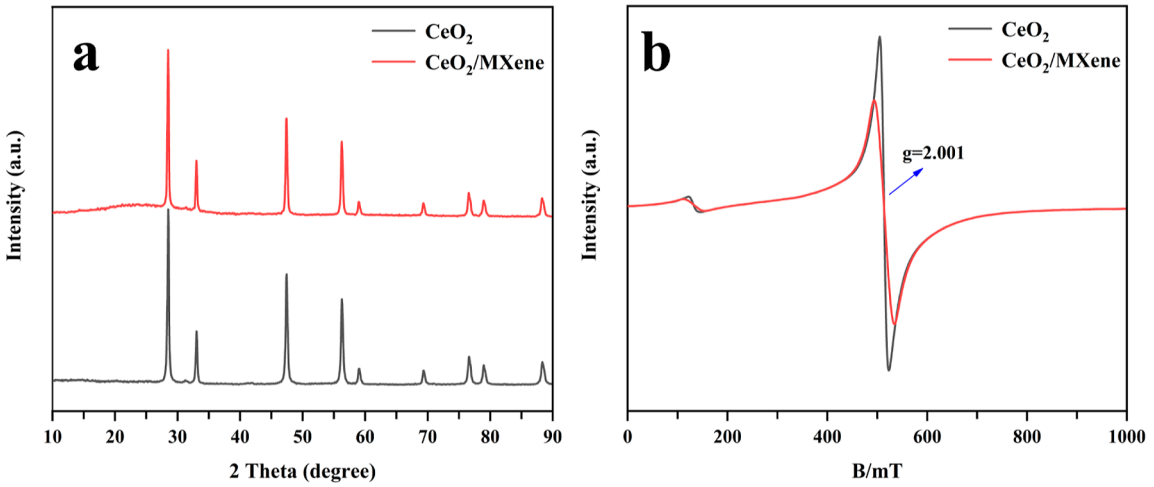

Figure 4. XRD patterns of (a) CeO_2 and CeO_2/MXene and (b) EPR signals of CeO_2 and CeO_2/MXene.

and a specific concentration of MXene nanosheet suspension were mixed in a beaker, stirred for 30 min, washed with distilled water, centrifuged several times, and dried in vacuum for 12 h. Finally, the CeO_2/MXene solid powder catalyst can be obtained.

3. RESULTS AND DISCUSSION

The preparation method of the CeO_2/MXene catalyst is illustrated in Scheme 1, and the specific steps are shown in Section 2.4. Zeta potential measurements determined the surface charge properties of CeO_2 and MXene. As indicated in Figure S1, the zeta potential value of MXene is −31.05 mV, which suggests that the MXene surface is negatively charged, while the zeta potential value of pure CeO_2 is 46.03 mV. Therefore, the 3D/2D CeO_2/MXene heterostructure can be formed by electrostatic interaction self-assembly between CeO_2 and MXene.

The SEM images show that the synthesized CeO_2 presents an octahedral shape with an occasional texture on the surface, forming nanorod-like arms with a length of about 150 nm (Figure 1a–d). The synthesized nanocrystals have a uniform morphology and a particle size of about 500–600 nm. The facet-based homojunction formed on the surface of CeO_2 nanocrystals provides more active sites for photocatalytic reactions.[24] Supplementary SEM images are shown in Figure S2.

The morphology and thickness of the prepared Ti_3C_2 were observed using a field emission transmission electron microscope and an atomic force microscope. As shown in AFM images and the corresponding height profiles in Figure 2a–c, Ti_3C_2 has a typical nanosheet-like morphology with a thickness of about 4.35 nm). Meanwhile, Figure 2d,e shows that the Ti_3C_2 MXene has a typical sheet shape with slight wrinkles on the edges. The unetched MXene can be seen in Figure S2, which is many times thicker than the etched MXene layer and

https://doi.org/10.1021/acsomega.2c01674
ACS Omega 2022, 7, 21684−21693

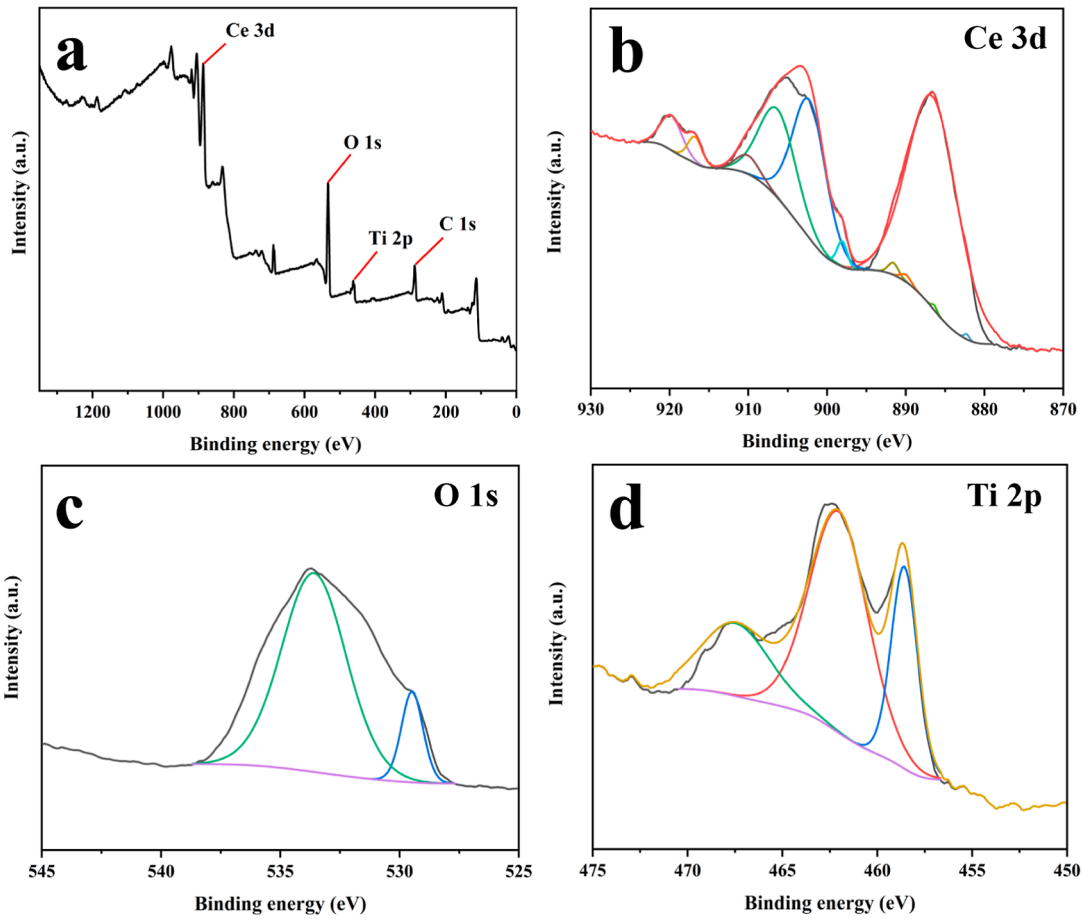

Figure 5. Full spectrum (a) and high-resolution XPS spectra of Ce 3d (b), O 1S (c), and Ti 2p (d).

is not conducive to the transport of photogenerated charges. The exfoliated nanosheets can also have the optical path length significantly reduced, the photoexcitation range increased, and the bandgap value reduced. The TEM images of MXene without HF etching are shown in Figure S3.

The synthesis conditions of CeO_2/Ti_3C_2 nanocomposites are simple, mild, and easily reproducible. SEM images in Figures 3a–d and S4a–f prove that the MXene material covers the surface of CeO_2, and the Mxene material is thin and has a smooth surface. The contact area between MXene and CeO_2 is relatively wide and conducive to the transfer of photogenerated carriers. The TEM image in Figure 3e further confirms the formation of the 3D/2D heterojunction. Moreover, there is no obvious MXene material on the surface of CeO_2.[26] This is due to the ultra-thin layer spacing of MXene which causes the morphology to be not clearly shown in TEM images. The corresponding enlarged images (Figures 3h and S5c) show the different interfaces between CeO_2 and MXene, and the staggering lattice fringes prove that the heterojunction is formed between CeO_2 and MXene. Therefore, the SEM and TEM results show that CeO_2 and MXene are easy to composite. Consistent with this, the HAADF images of the sample (Figures 3i and S6) indicate that the material contains all elements such as Ce, O, C, and Ti.

As shown in Figure 4a, the crystal structure of the synthesized material was analyzed by XRD. The typical diffraction peaks at 2θ = 28.55, 33.08, 47.48, and 56.33 correspond to CeO_2 (111), (200), (220), and (311) planes, respectively, by comparing with the standard card (JCPDS 34-0394).[27,28] The XRD pattern of CeO_2/MXene showed that the XRD peaks did not change much after MXene was compounded, which proved that the crystal structure of CeO_2 did not change significantly. It may that the ultrathin characteristics of MXene led to the little XRD diffraction peaks.[29] The removed O-terminus on the surface of MXene may lead to the formation of O vacancies, and after recombination with CeO_2, the concentration of O vacancies may increase, and the peak value of the EPR signal may become higher. The existence of oxygen defects in CeO_2 is demonstrated by electron paramagnetic resonance spectroscopy, and pure CeO_2 exhibits an insignificant symmetry signal at g = 2.001, which is due to the capture of unpaired electrons on the oxygen defects.[30,31] Such oxygen vacancies can more effectively separate photo-generated electron–hole pairs, resulting in good photocatalytic activity of the material.[32] After complexation with MXene, the signal peak becomes more intense, implying an increase in the concentration of oxygen vacancies, which may be because MXene itself contains specific oxygen vacancies.[33]

The XPS technology was used to study the surface chemical composition and the valence state of the CeO_2/MXene composites. The Ce 3d spectrum (Figure 5b) can be fitted with eight peaks at 884.3, 884.2, 887.5, 893.6, 898.7, 902.4, 907.3, and 916.4 eV, which can be divided into two groups of spin–orbit multiplets representing Ce 3d3/2 and Ce 3d2/5. u and υ bands are from Ce^{3+}. In contrast, the other bands are attributed to Ce^{4+}.[28,34] The presence of the Ce^{3+}/Ce^{4+} oxidation state mixture on the CeO_2/MXene surface indicates

https://doi.org/10.1021/acsomega.2c01674
ACS Omega 2022, 7, 21684–21693

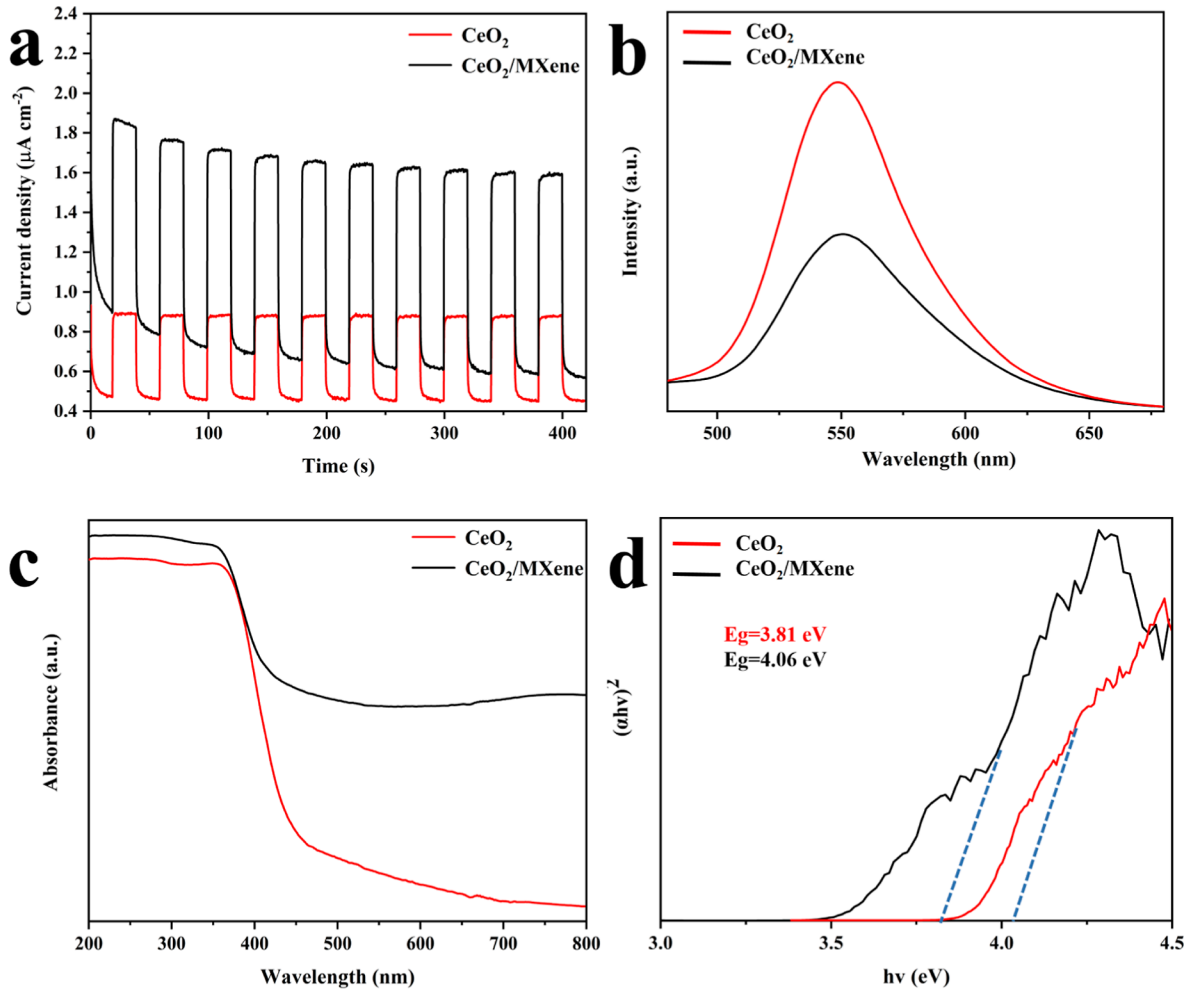

Figure 6. (a) Transient photocurrent, (b) PL spectra, (c) UV−vis DRS spectra, and (d) Tauc's plots.

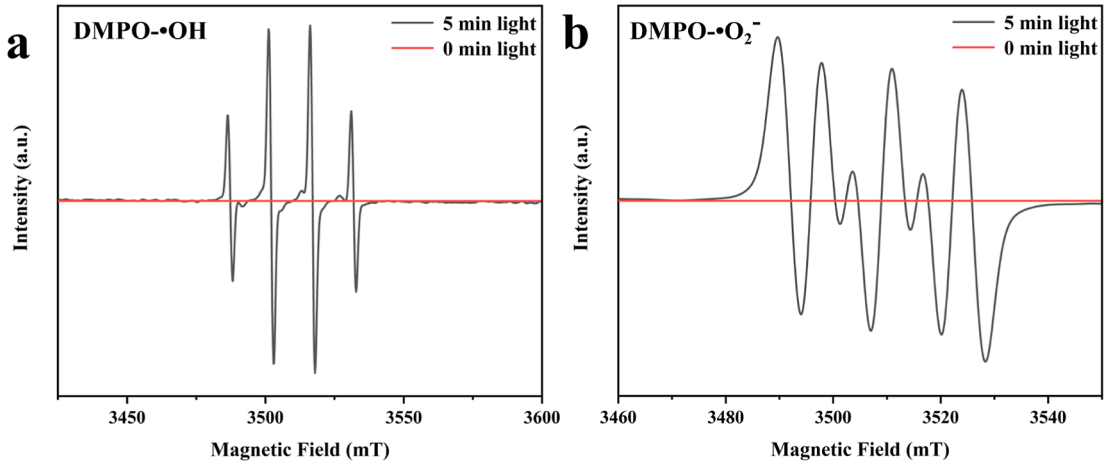

Figure 7. (a) DMPO spin-trapping ESR spectra of CeO_2/MXene in methanol dispersion for DMPO-•O_2^- and (b) aqueous dispersion for DMPO-•OH.

that the oxidation state may not be fully formed on the sample surface, which may be caused by the oxygen vacancies present in the CeO_2 crystal structure. The O 1s spectra of CeO_2 and CeO_2/MXene (Figure 5c) are observed at peaks of 529.3 and 531.6 eV, respectively. The lower binding energy (BES) peaks are considered to be due to the Ce−O bonds, while the higher peaks are considered to be due to the surface-adsorbed oxygen and H_2O.[27,35] As shown in Figure 5d, the two peaks in the Ti 2p XPS spectra at 458.6 and 462.09 eV are attributed to the Ti−C bond, while two peaks at 467.64 eV are attributed to the Ti−O bond, which come from the surface attached oxygen-containing functional groups on MXene.[6] The C 1s spectra of MXene can be fitted into four peaks located at 281.3, 284.8, 286.7, and 288.6 eV which are assigned to C−Ti, C−C, C−O,

https://doi.org/10.1021/acsomega.2c01674
ACS Omega 2022, 7, 21684−21693

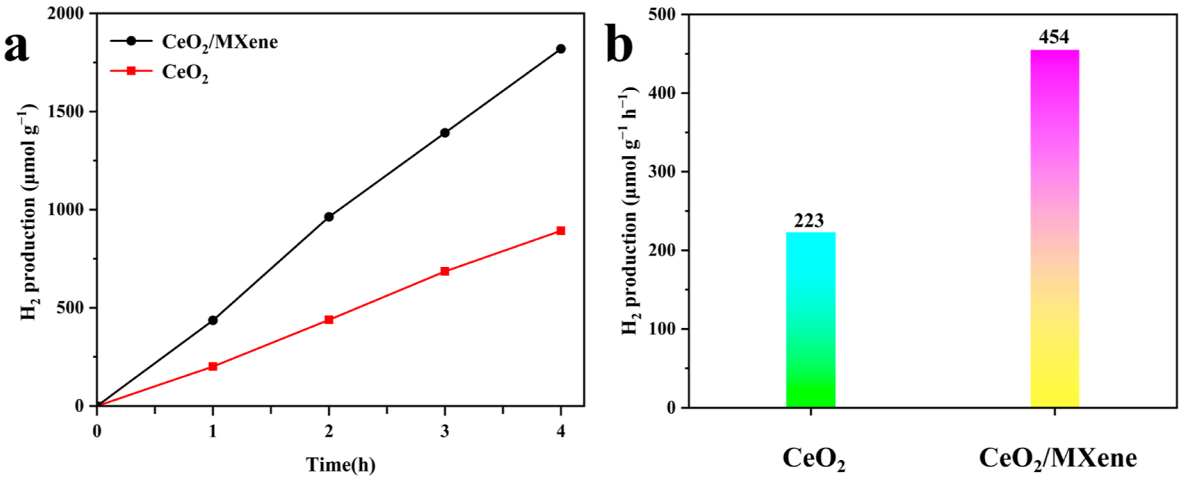

Figure 8. (a) Time-dependent H_2 evolution. (b) H_2 evolution rate of CeO_2 and CeO_2/MXene.

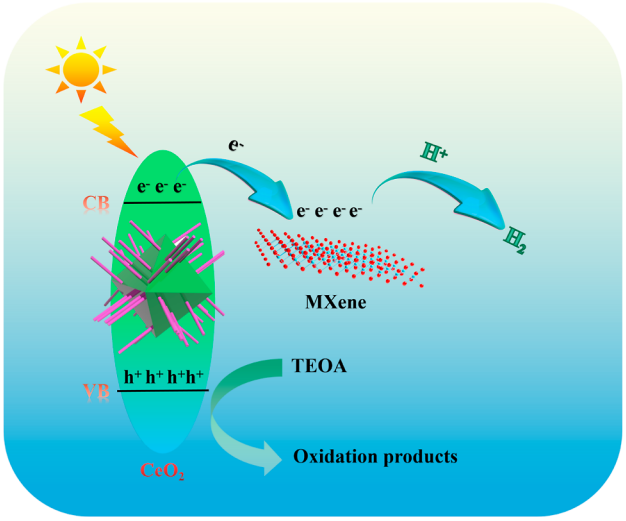

Figure 9. Schematic diagram of possible electron transfer paths and photocatalytic H_2 evolution mechanism in CeO_2/MXene.

and C−F bonds, respectively, and the spectra are shown in Figure S7.[36]

Figure 6a shows the transient photocurrent responses of CeO_2 and CeO_2/MXene samples. By comparing the photocurrent densities of different samples, it is proved that CeO_2/MXene has almost 1.25 times higher photocurrent density than CeO_2, which indicates that the photo-generated carrier transfer rate can be significantly enhanced after compositing MXene.[23] The excellent electrical conductivity of MXene makes the photoluminescence intensity of CeO_2/MXene the weakest in the photoluminescence spectrum (Figure 6b), indicating that CeO_2/MXene has the best electron−hole separation performance.[37] The light absorption properties of the synthesized materials were tested by the UV−vis DRS technique, as shown in Figure 6. According to Figure 6c, pure CeO_2 has a clear absorption spectrum in the visible range (390−780 nm). At the same time, CeO_2/MXene samples' absorption spectrum begins to red shift, indicating that MXene helps increase the capacity of light absorption. The samples' electron transfer path and valence band position can be better studied by calculating the indirect band energy from the ultraviolet spectrum. The corresponding band gap energies were calculated from the Kubelka−Munk function $\alpha h\nu = A\ (h\nu - E_g)^{1/2}$, based on the tangent lines of $(\alpha h\nu)^2$ to $h\nu$ plots, where α is the absorption coefficient and $h\nu$ is the photon energy. Figure 6d presents Tauc's plot for estimating the corresponding band gap energy (E_g). The E_g values of pure CeO_2 and CeO_2/MXene were calculated to be 3.81 and 4.06 eV, respectively, by linear extrapolation.[38] Compared with CeO_2, the band gap of CeO_2/MXene is obviously narrowed, which means that light can be more easily excited to promote the transfer of photo-generated electrons on the surface of the CeO_2/MXene sample, thus making CeO_2/MXene show better photocatalytic performance.[39,40] The valence band positions of the catalysts were analyzed using the VB-XPS spectra (Figure S8) and were 2.16 and 2.08 eV for CeO_2 and CeO_2/Mxene, respectively. The conduction band positions were −1.9 and −1.73 eV, respectively, calculated using the $E_{CB} = E_{VB} - E_g$ equation.

Figure 7a,b shows that CeO_2/MXene does not show DMPO-•O_2^- or DMPO-•OH signals under dark conditions, which indicates that photocatalytic reactions will not occur under conditions of no light. After 5 min of visible light irradiation, an unmistakable response signal of DMPO-•OH was detected. It proves two points: first, •OH and •O_2^- will be produced during the photocatalytic reaction. Second, as the illumination time increases, the signal becomes more intense, proving that the concentration of free radicals increases.[41,42]

The samples were also used in a photocatalytic H_2 evolution experiment to verify further the effect of a photo-generated electron in practical applications. The photocatalytic hydrogen evolution (PHE) performance with different catalysts is presented in Figure 8a,b. The results show that the PHE rate of CeO_2/MXene is 454.32 μmol·g^{-1}·h^{-1}, while that of CeO_2 is 223.15 μmol·g^{-1}·h^{-1}. Compared with CeO_2, the PHE rate of CeO_2/MXene is more than doubled. Because MXene's efficient electron transfer capability, it may be that protons react more quickly with light-generated electrons to produce more H_2. Meanwhile, the hydrogen evolution results show that MXene can effectively enhance the activity of photocatalysts. Figure S9 shows continuous H_2 production with no noticeable decrease in the subsequent reactions, demonstrating that the synthesized material is reusable.

We propose a possible PHE mechanism based on these experimental and theoretical data (Figure 9). First, MXene can form a heterojunction structure after being combined on the CeO_2 surface. When the electrons in CeO_2 are excited, the

https://doi.org/10.1021/acsomega.2c01674
ACS Omega 2022, 7, 21684−21693

photo-generated electrons are first excited and jump from the valence band to the conduction band. Due to the smooth surface structure and excellent interlayer structure of MXene, photoexcited electrons can migrate rapidly from semiconductor CeO_2 to metallic MXene through the tightly coupled interface. Meanwhile, the photo-generated holes remaining in the valence band of CeO_2 are consumed by the sacrificial agent. Subsequently, photo-generated electrons are further reacted with the absorbed protons under light to produce H_2.[43−46]

4. CONCLUSIONS

In summary, we successfully prepared 3D CeO_2/2D Ti_3C_2 MXene photocatalysts by compositing ultrathin exfoliated Ti_3C_2 MXene nanosheets on the CeO_2 surface. The constructed 3D/2D CeO_2/MXene structures have excellent interfacial effects, desirable photoresponsive properties, and high photo-generated carrier mobility. The process of photocatalytic hydrogen precipitation under light illumination can be realized by adding a small amount of CeO_2/MXene photocatalyst. The experimental results show that the special two-dimensional structure, fast carrier migration rate, and ideal interfacial effects of Ti_3C_2 MXene have unique synergistic effects on photocatalytic H_2 evolution. The Schottky contact between the n-type semiconductor CeO_2 and the metal-like Ti_3C_2 can significantly promote the separation of photo-generated carriers and the transfer of the photo-generated electrons to MXene nanosheets, endowing the Schottky heterojunction with strong photocatalytic activity, which can be used for the photocatalytic H_2 evolution process. The construction of heterojunction photocatalytic systems is an effective way to enhance photocatalytic performance because 2D semiconductors can act as electron acceptors to improve charge separation and prolong the carrier lifetime. In addition, the semiconductor material CeO_2 transferred the photo-generated electrons to Mxene, which accelerated the reduction rate of protons to produce more hydrogen gas and improved the photocatalytic performance. It provides a new idea for fabricating rare earth metal oxide and 2D MXene composites and can be applied to other similar 3D/2D heterostructures.

■ ASSOCIATED CONTENT

Supporting Information

The Supporting Information is available free of charge at https://pubs.acs.org/doi/10.1021/acsomega.2c01674.

Supplementary experimental section; zeta potentials; supplementary SEM and TEM images; C 1s XPS spectra; and VB-XPS spectra (PDF)

■ AUTHOR INFORMATION

Corresponding Author

Hongrui Zhu − *College of Chemistry and Chemical Engineering, Lanzhou Jiaotong University, Lanzhou, Gansu 730070, P. R. China;* orcid.org/0000-0001-8449-1748; Email: zhuhongrui0124@163.com

Authors

Xumei Fu − *College of Chemistry and Chemical Engineering, Lanzhou Jiaotong University, Lanzhou, Gansu 730070, P. R. China*

Zhiqiang Zhou − *College of Chemistry and Chemical Engineering, Xi'an Shiyou University, Xi'an, Shaanxi 3710065, P. R. China*

Complete contact information is available at: https://pubs.acs.org/10.1021/acsomega.2c01674

Author Contributions

H.Z., Z.Z. and X.F. conceived the study and designed the experiments, synthesis, and characterization. Electron microscopy and spectroscopy were performed and analyzed by H.Z.

Notes

The authors declare no competing financial interest.

■ ACKNOWLEDGMENTS

We thank Lanzhou Petrochemical Synthetic Rubber Plant for funding this paper and the Lanzhou Institute of Chemical Physics for their help with this paper.

■ REFERENCES

(1) Nishiyama, H.; Yamada, T.; Nakabayashi, M.; Maehara, Y.; Yamaguchi, M.; Kuromiya, Y.; Nagatsuma, Y.; Tokudome, H.; Akiyama, S.; Watanabe, T.; Narushima, R.; Okunaka, S.; Shibata, N.; Takata, T.; Hisatomi, T.; Domen, K. Photocatalytic solar hydrogen production from water on a 100-m2 scale. *Nature* **2021**, *598*, 304−307.

(2) Guo, M.; Xing, Z.; Zhao, T.; Qiu, Y.; Tao, B.; Li, Z.; Zhou, W. Hollow flower-like polyhedral α-Fe2O3/Defective MoS2/Ag Z-scheme heterojunctions with enhanced photocatalytic-Fenton performance via surface plasmon resonance and photothermal effects. *Appl. Catal., B* **2020**, *272*, 118978.

(3) Liu, G.; Kolodziej, C.; Jin, R.; Qi, S.; Lou, Y.; Chen, J.; Jiang, D.; Zhao, Y.; Burda, C. MoS2-Stratified CdS-Cu2-xS Core-Shell Nanorods for Highly Efficient Photocatalytic Hydrogen Production. *ACS Nano* **2020**, *14*, 5468−5479.

(4) Lan, K.; Wang, R.; Wei, Q.; Wang, Y.; Hong, A.; Feng, P.; Zhao, D. Stable Ti 3+ Defects in Oriented Mesoporous Titania Frameworks for Efficient Photocatalysis. *Angew. Chem., Int. Ed.* **2020**, *132*, 17829−17836.

(5) Li, C.; Ding, G.; Liu, X.; Huo, P.; Yan, Y.; Yan, Y.; Liao, G. Photocatalysis over NH2-UiO-66/CoFe2O4/CdIn2S4 double p-n junction: Significantly promoting photocatalytic performance by double internal electric fields. *Chem. Eng. J.* **2022**, *435*, 134740.

(6) Zeng, H.; Li, Z.; Li, G.; Cui, X.; Jin, M.; Xie, T.; Liu, L.; Jiang, M.; Zhong, X.; Zhang, Y.; Zhang, H.; Ba, K.; Yan, Z.; Wang, Y.; Song, S.; Huang, K.; Feng, S. Interfacial Engineering of TiO 2 /Ti 3 C 2 MXene/Carbon Nitride Hybrids Boosting Charge Transfer for Efficient Photocatalytic Hydrogen Evolution. *Adv. Energy Mater.* **2021**, *12*, 2102765.

(7) Hao, C.-c.; Tang, Y.-b.; Shi, W.-l.; Chen, F.-y.; Guo, F. Facile solvothermal synthesis of a Z-Scheme 0D/3D CeO2/ZnIn2S4 heterojunction with enhanced photocatalytic performance under visible light irradiation. *Chem. Eng. J.* **2021**, *409*, 128168.

(8) Zhang, J.; Shan, Q.; Feng, H.; Hu, T.; Wu, Y.; Luo, T.; Tang, W.; Wang, D. Efficient degradation of tetracycline using core−shell Fe@Fe_2O_3-CeO_2 composite as novel heterogeneous electro-Fenton catalyst. *Chem. Eng. J.* **2022**, *428*, 131403.

(9) Jin, X.; Duan, Y.; Liu, D. P.; Feng, X. L.; Li, W.; Zhang, Z.; Zhang, Y. CO Oxidation Catalyzed by Two-Dimensional Co_3O_4/CeO_2 Nanosheets. *ACS Appl. Nano Mater.* **2019**, *2*, 5769−5778.

(10) Wang, F.; Wang, X.; Liu, D.; Zhen, J.; Li, J.; Wang, Y.; Zhang, H. High-Performance ZnCo2O4@CeO2 Core@shell Microspheres for Catalytic CO Oxidation. *ACS Appl. Mater. Interfaces* **2014**, *6*, 22216−22223.

(11) Amoresi, R. A. C.; Oliveira, R. C.; Marana, N. L.; de Almeida, P. B.; Prata, P. S.; Zaghete, M. A.; Longo, E.; Sambrano, J. R.; Simões, A. Z. CeO2 Nanoparticle Morphologies and Their Corresponding

Crystalline Planes for the Photocatalytic Degradation of Organic Pollutants. *ACS Appl. Nano Mater.* **2019**, *2*, 6513−6526.
(12) Li, C.; Sun, Y.; Djerdj, I.; Voepel, P.; Sack, C.-C.; Weller, T.; Ellinghaus, R.; Sann, J.; Guo, Y.; Smarsly, B. M.; Over, H. Shape-Controlled CeO2 Nanoparticles: Stability and Activity in the Catalyzed HCl Oxidation Reaction. *ACS Catal.* **2017**, *7*, 6453−6463.
(13) Jiang, D.; Wang, W.; Zhang, L.; Zheng, Y.; Wang, Z. Insights into the Surface-Defect Dependence of Photoreactivity over CeO2 Nanocrystals with Well-Defined Crystal Facets. *ACS Catal.* **2015**, *5*, 4851−4858.
(14) Zheng, X.; Li, Y.; Zhang, L.; Shen, L.; Xiao, Y.; Zhang, Y.; Au, C.; Jiang, L. Insight into the effect of morphology on catalytic performance of porous CeO2 nanocrystals for H2S selective oxidation. *Appl. Catal., B* **2019**, *252*, 98−110.
(15) Xu, X.; Zhang, Y.; Sun, H.; Zhou, J.; Yang, F.; Li, H.; Chen, H.; Chen, Y.; Liu, Z.; Qiu, Z.; Wang, D.; Ma, L.; Wang, J.; Zeng, Q.; Peng, Z. Progress and Perspective: MXene and MXene-Based Nanomaterials for High-Performance Energy Storage Devices. *Adv. Electron. Mater.* **2021**, *7*, 2000967.
(16) Zuo, G.; Wang, Y.; Teo, W. L.; Xie, A.; Guo, Y.; Dai, Y.; Zhou, W.; Jana, D.; Xian, Q.; Dong, W.; Zhao, Y. Ultrathin ZnIn 2 S 4 Nanosheets Anchored on Ti 3 C 2 T X MXene for Photocatalytic H 2 Evolution. *Angew. Chem., Int. Ed.* **2020**, *59*, 11287−11292.
(17) Kuang, P.; Low, J.; Cheng, B.; Yu, J.; Fan, J. MXene-based photocatalysts. *J. Mater. Sci. Technol.* **2020**, *56*, 18.
(18) You, Z.; Liao, Y.; Li, X.; Fan, J.; Xiang, Q. State-of-the-art recent progress in MXene-based photocatalysts: a comprehensive review. *Nanoscale* **2021**, *13*, 9463−9504.
(19) Liu, J.; Fu, W.; Liao, Y.; Fan, J.; Xiang, Q. Recent advances in crystalline carbon nitride for photocatalysis. *J. Mater. Sci. Technol.* **2021**, *91*, 224.
(20) Zhang, R.; Dong, J.; Zhang, W.; Ma, L.; Jiang, Z.; Wang, J.; Huang, Y. Synergistically coupling of 3D FeNi-LDH arrays with Ti_3C_2Tx-MXene nanosheets toward superior symmetric supercapacitor. *Nano Energy* **2022**, *91*, 106633.
(21) Chertopalov, S.; Mochalin, V. N. Environment-Sensitive Photoresponse of Spontaneously Partially Oxidized Ti3C2 MXene Thin Films. *ACS Nano* **2018**, *12*, 6109−6116.
(22) Yun, T.; Lee, G. S.; Choi, J.; Kim, H.; Yang, G. G.; Lee, H. J.; Kim, J. G.; Lee, H. M.; Koo, C. M.; Lim, J.; Kim, S. O. Multidimensional Ti3C2Tx MXene Architectures via Interfacial Electrochemical Self-Assembly. *ACS Nano* **2021**, *15*, 10058−10066.
(23) Li, J.-Y.; Li, Y.-H.; Zhang, F.; Tang, Z.-R.; Xu, Y.-J. Visible-light-driven integrated organic synthesis and hydrogen evolution over 1D/2D CdS-Ti3C2Tx MXene composites. *Appl. Catal., B* **2020**, *269*, 118783.
(24) Li, P.; Zhou, Y.; Zhao, Z.; Xu, Q.; Wang, X.; Xiao, M.; Zou, Z. Hexahedron Prism-Anchored Octahedronal CeO2: Crystal Facet-Based Homojunction Promoting Efficient Solar Fuel Synthesis. *J. Am. Chem. Soc.* **2015**, *137*, 9547−9550.
(25) Cui, C.; Cheng, R.; Zhang, H.; Zhang, C.; Ma, Y.; Shi, C.; Fan, B.; Wang, H.; Wang, X. Ultrastable MXene@Pt/SWCNTs' Nano-catalysts for Hydrogen Evolution Reaction. *Adv. Funct. Mater.* **2020**, *30*, 2000693.
(26) Zuo, G.; Wang, Y.; Teo, W.; Xie, A.; Guo, Y.; Dai, Y.; Zhou, W.; Jana, D.; Xian, Q.; Dong, W.; Zhao, Y. Ultrathin $ZnIn_2S_4$ Nanosheets Anchored on Ti_3C_2TX MXene for Photocatalytic H_2 Evolution. *Angew. Chem., Int. Ed.* **2020**, *132*, 11287−11292.
(27) Wang, A.; Zheng, Z.; Wang, H.; Chen, Y.; Luo, C.; Liang, D.; Hu, B.; Qiu, R.; Yan, K. 3D hierarchical H2-reduced Mn-doped CeO2 microflowers assembled from nanotubes as a high-performance Fenton-like photocatalyst for tetracycline antibiotics degradation. *Appl. Catal., B* **2020**, *277*, 119171.
(28) Zhang, S.; Wang, H.; Si, H.; Jia, X.; Wang, Z.; Li, Q.; Kong, J.; Zhang, J. Novel Core-Shell (ε-MnO2/CeO2)@CeO2 Composite Catalyst with a Synergistic Effect for Efficient Formaldehyde Oxidation. *ACS Appl. Mater. Interfaces* **2020**, *12*, 40285−40295.
(29) Cao, S.; Shen, B.; Tong, T.; Fu, J.; Yu, J. 2D/2D Heterojunction of Ultrathin MXene/Bi2 WO6 Nanosheets for Improved Photocatalytic CO2 Reduction. *Adv. Funct. Mater.* **2018**, *28*, 1800136.
(30) Jiao, X.; Chen, Z.; Li, X.; Sun, Y.; Gao, S.; Yan, W.; Wang, C.; Zhang, Q.; Lin, Y.; Luo, Y.; Xie, Y. Defect-Mediated Electron-Hole Separation in One-Unit-Cell ZnIn2S4 Layers for Boosted Solar-Driven CO2 Reduction. *J. Am. Chem. Soc.* **2017**, *139*, 7586−7594.
(31) Spanopoulos, I.; Hadar, I.; Ke, W.; Guo, P.; Mozur, E. M.; Morgan, E.; Wang, S.; Zheng, D.; Padgaonkar, S.; Manjunatha Reddy, G. N.; Weiss, E. A.; Hersam, M. C.; Seshadri, R.; Schaller, R. D.; Kanatzidis, M. G. Tunable Broad Light Emission from 3D "Hollow" Bromide Perovskites through Defect Engineering. *J. Am. Chem. Soc.* **2021**, *143*, 7069−7080.
(32) Dai, Z.; Qin, F.; Zhao, H.; Ding, J.; Liu, Y.; Chen, R. Crystal Defect Engineering of Aurivillius Bi2MoO6 by Ce Doping for Increased Reactive Species Production in Photocatalysis. *ACS Catal.* **2016**, *6*, 3180−3192.
(33) Tang, Y.; Yang, C.; Xu, X.; Kang, Y.; Henzie, J.; Que, W.; Yamauchi, Y. MXene Nanoarchitectonics: Defect-Engineered 2D MXenes towards Enhanced Electrochemical Water Splitting. *Adv. Energy Mater.* **2022**, *12*, 2103867.
(34) Ma, R.; Zhang, S.; Li, L.; Gu, P.; Wen, T.; Khan, A.; Li, S.; Li, B.; Wang, S.; Wang, X. Enhanced Visible-Light-Induced Photoactivity of Type-II CeO2/g-C3N4 Nanosheet toward Organic Pollutants Degradation. *ACS Sustainable Chem. Eng.* **2019**, *7*, 9699−9708.
(35) Wei, L.; Liu, Y.; Dai, H.; Cui, S.; Wang, C.; Hsi, H.-C.; Duan, E.; Peng, Y.; Deng, J. Electronic structure tailoring of Al3+- and Ta5+-doped CeO2 for the synergistic removal of NO and chlorinated organics. *Appl. Catal., B* **2022**, *304*, 120939.
(36) Xiao, R.; Zhao, C.; Zou, Z.; Chen, Z.; Tian, L.; Xu, H.; Tang, H.; Liu, Q.; Lin, Z.; Yang, X. In situ fabrication of 1D CdS nanorod/2D Ti3C2 MXene nanosheet Schottky heterojunction toward enhanced photocatalytic hydrogen evolution. *Appl. Catal., B* **2020**, *268*, 118382.
(37) Tang, H.; Feng, H.; Wang, H.; Wan, X.; Liang, J.; Chen, Y. Highly Conducting MXene-Silver Nanowire Transparent Electrodes for Flexible Organic Solar Cells. *ACS Appl. Mater. Interfaces* **2019**, *11*, 25330−25337.
(38) Yang, C.; Tan, Q.; Li, Q.; Zhou, J.; Fan, J.; Li, B.; Sun, J.; Lv, K. 2D/2D Ti3C2 MXene/g-C3N4 nanosheets heterojunction for high efficient CO2 reduction photocatalyst: Dual effects of urea. *Appl. Catal., B* **2020**, *268*, 118738.
(39) Zhao, M. Q.; Xie, X.; Ren, C. E.; Makaryan, T.; Anasori, B.; Wang, G.; Gogotsi, Y. Hollow MXene Spheres and 3D Macroporous MXene Frameworks for Na-Ion Storage. *Adv. Mater.* **2017**, *29*, 1702410.
(40) Han, K.; Wang, Y.; Wang, S.; Liu, Q.; Deng, Z.; Wang, F. Narrowing band gap energy of CeO2 in (Ni/CeO2)@SiO2 catalyst for photothermal methane dry reforming. *Chem. Eng. J.* **2021**, *421*, 129989.
(41) Fei, H.; Shao, J.; Li, H.; Li, N.; Chen, D.; Xu, Q.; He, J.; Lu, J. Construction of ultra-thin 2D CN-Br0.12/2%RhOx photo-catalyst with rapid electron and hole separation for efficient bisphenol A degradation. *Appl. Catal., B* **2021**, *299*, 120623.
(42) Xu, H.; She, X.; Fei, T.; Song, Y.; Liu, D.; Li, H.; Yang, X.; Yang, J.; Li, H.; Song, L.; Ajayan, P. M.; Wu, J. Metal-Oxide-Mediated Subtractive Manufacturing of Two-Dimensional Carbon Nitride for High-Efficiency and High-Yield Photocatalytic H2 Evolution. *ACS Nano* **2019**, *13*, 11294−11302.
(43) Ran, J.; Guo, W.; Wang, H.; Zhu, B.; Yu, J.; Qiao, S. Z. Metal-Free 2D/2D Phosphorene/g-C 3 N 4 Van der Waals Heterojunction for Highly Enhanced Visible-Light Photocatalytic H 2 Production. *Adv. Mater.* **2018**, *30*, 1800128.
(44) Li, R.; Zhang, L.; Shi, L.; Wang, P. MXene Ti3C2: An Effective 2D Light-to-Heat Conversion Material. *ACS Nano* **2017**, *11*, 3752−3759.
(45) Li, C.; Liu, X.; Huo, P.; Yan, Y.; Liao, G.; Ding, G.; Liu, C. Boosting H 2 Production over C 60 -Mediated NH 2 -MIL-125(Ti)/Zn 0.5 Cd 0.5 S S-Scheme Heterojunction via Enhanced Interfacial Carrier Separation. *Small* **2021**, *17*, 2102539.

https://doi.org/10.1021/acsomega.2c01674
ACS Omega 2022, 7, 21684−21693

(46) Li, C.; Liu, X.; Ding, G.; Huo, P.; Yan, Y.; Yan, Y.; Liao, G. Interior and Surface Synergistic Modifications Modulate the SnNb2O6/Ni-Doped ZnIn2S4 S-Scheme Heterojunction for Efficient Photocatalytic H2 Evolution. *Inorg. Chem.* **2022**, *61*, 4681−4689.

https://doi.org/10.1021/acsomega.2c01674
ACS Omega 2022, 7, 21684−21693